J. Fluid Mech. (1983), *vol.* 127, *pp.* 379–401
Printed in Great Britain

Laterally converging flow. Part 1. Mean flow

By H. D. MURPHY,
University of California, Los Alamos National Laboratory, NM 87545

F. W. CHAMBERS†
University of New Mexico, Albuquerque, NM 87131

AND D. M. McELIGOT
University of Arizona, Tucson, AZ 85721

(Received 11 August 1981 and in revised form 5 May 1982)

Laterally converging flow occurs between two parallel surfaces with an exit hole formed in one. The present study examines the flow at a distance from the exit as a means of investigating an accelerating radial internal flow induced by the lateral convergence and satisfying the boundary-layer approximations. The measurements range from laminar to turbulent conditions, including the intermediate stage referred to by some investigators as laminarizing or laminarescent. The acceleration parameter $K_V = (\nu/V^2)\,dV/dr$ ranges from $2{\cdot}6\times10^{-8}$ to $2{\cdot}2\times10^{-4}$ and the local Reynolds number varies from 210 to $6{\cdot}8\times10^4$ for the data reported; the relation between the Reynolds number and the acceleration parameter was varied by adjusting the convergence angle or the plate spacing. For the main experiment the accelerating region is 86 plate spacings in length. Comparison with numerical predictions for laminar and turbulent flow leads to identification of flow regimes in terms of popular acceleration parameters K_V, $K_p = (\nu/\rho u_*^3)\,dp/dr$ and $K_\tau = (\nu/\rho u_*^3)\,(\partial\tau/\partial z)_w$. Results demonstrate that a potentially turbulent entry flow subjected to accleration due to lateral convergence shows features common to laminarization in accelerating turbulent boundary layers in other geometries. Application of the function $A^+(K_p)$ for a modified van Driest wall-region model is examined briefly for the intermediate regime.

1. Introduction

This paper is one describing a 'complex' turbulent flow (Bradshaw 1975, 1976). In the present case the shear layer is influenced by the extra rate of strain and the streamwise acceleration associated with lateral convergence and by interaction with an identical turbulence field propagated from a second surface parallel to the test surface. In some aspects the flow is the counterpart of the lateral divergence examined by Smits, Eaton & Bradshaw (1979) but the apparatus and range of strain-rate ratios differ considerably. The main interest focuses on the effects in the near-wall region, which usually dominates heat and mass transfer, erosion, wall shear stress and pressure drop, while a secondary, related concern is the treatment of the empirical constants required in simple calculation methods as by Launder & Jones (1969) and Huffman & Bradshaw (1972). Such calculations are usually required to provide

† Present address: Lockheed-Georgia Company, Marietta, GA 30063.

boundary conditions – or wall functions – for most higher-order turbulence models.

While the details of many accelerating flows have been extensively studied (Narasimha & Sreenivasan 1979; Murphy 1979), this appears to be the first investigation of turbulent flow accelerating owing to lateral convergence between parallel plates. The idealized axisymmetric geometry and coordinate system are demonstrated in figure 1; the study is confined to the region sufficiently far away from the tubular exit so that boundary-layer assumptions for internal flows remain valid. The apparatus, mean measurements and comparison to predictions are provided in the present paper, while temporal measurements of the fluctuating wall shear stress are presented in the companion paper, part 2 (Chambers, Murphy & McEligot 1983).

In the idealized problem the velocity is uniform at an entry at a large radius. The flow develops and may approach a fully established profile. At small radii, acceleration dominates the flow in the centre of the duct, causing a flattening of the profile. The profile takes the appearance of an external boundary-layer flow, with a large central core flanked on both sides with thin boundary layers. The boundary layers become successively thinner as acceleration continues. Depending on the entering radius and flow rate, the regime may be laminar or turbulent, or an initially turbulent flow may approach a laminar flow owing to the stabilizing effects of acceleration, i.e. 'laminarization' may occur.

The facility employed in the present work differs from those used previously to study laminarization in that it has a long test section along which the acceleration can be applied continuously. Further, both Reynolds numbers and acceleration parameters can be varied over large ranges.

Several authors have proposed various non-dimensional parameters involving either velocity, pressure or shear-stress gradients which purportedly serve as a guide to the likelihood of laminarization. Kline *et al.* (1967) noticed that turbulent bursts ceased when an acceleration parameter $K_u = (\nu/u_\infty^2)\,du_\infty/dr$ reached a critical value of $3{\cdot}7 \times 10^{-6}$. Jones & Launder (1972) found that the peak Reynolds stress due to turbulence became a progressively smaller fraction of the wall shear stress as K_u increased. They indicated that, a turbulent flow could no longer exist when K_u exceeded a critical value somewhere between $2{\cdot}5 \times 10^{-6}$ and $3{\cdot}5 \times 10^{-6}$. Blackwelder & Kovasznay (1972) found that, when K_u exceeded the above critical values, the viscous-sublayer thickness increased, the skin-fraction coefficient at the wall decreased, and large departures from the turbulent logarithmic law of the wall occurred.

Patel (1965) also noted major departures from the logarithmic law, but correlated his results in terms of a pressure-gradient parameter $K_p = (\nu/\rho u_*^3)\,dp/dr$. Patel & Head (1968) suggested 0·018 for a critical value of K_p. They also suggested that a more appropriate laminarization parameter might be defined by replacing the pressure gradient with the shear stress gradient at the wall $(\partial\tau/\partial z)_w$; we shall call it K_τ. Since the gradient $\partial\tau/\partial z$ is evaluated at the wall, where the convective terms in the boundary-layer momentum equation are zero, $dp/dr = (\partial\tau/\partial z)_w$ for flow between parallel plates, whether fully developed or accelerating; for fully developed pipe flow $dp/dx = 2\,\partial\tau(y)/\partial y$. For transitional pipe flow Patel & Head found that with the present nomenclature $K_p = 2K_\tau = 0{\cdot}018$, whereas for transitional flow between parallel plates they found that $K_p = K_\tau = 0{\cdot}009$. On the basis of consistency, then, they concluded that K_τ was a better guide to the possibility of laminarization and that its critical value was 0·009 or so. They also suggested that the downstream distance required to reverse transition completely must be dependent upon the Reynolds number based on momentum thickness, $R_2 = u_\infty\,\delta_2/\nu$. Narasimha & Sreenivasan (1973) pointed out that the critical value of K_τ should have been 0·004, owing to

algebraic errors. They concluded that laminarization was due to domination of pressure gradients over the Reynolds stresses and therefore the parameter K_p incorporating the pressure gradient was recommended. In addition, they pointed out that parameters such as K_u, K_p and K_τ cannot be universally useful for all levels of acceleration. When the acceleration is very low, as in a nearly fully developed duct flow, the flow and its state of turbulence revert to their equilibrium values and the local Reynolds number then provides the best guide to the possibility of laminarization.

From measurement of the local Nusselt number in strongly heated gas flow in a circular tube, McEligot (1963) detected premature transition from turbulent flow towards laminar flow. He proposed the explanation to be a thickening of the viscous sublayer and correlated the flow regimes in terms of a non-dimensional heating rate and inlet Reynolds number. The correlation was later shown by McEligot, Coon & Perkins (1970) to be related to an acceleration parameter $K_V = (\nu/V^2)\,dV/dr$ based on the bulk velocity. This parameter K_V is a version of K_u appropriate for internal flows. Another Reynolds-number criterion was proposed by Bradshaw (1969), who postulated that a turbulent flow would become directly dependent upon viscosity, i.e. laminarizing, when the energy-containing and the dissipation ranges of eddy size overlap. This led to a critical 'eddy' Reynolds number $R_{\text{eddy}} = u_* L/\nu = 12$, where L is the dissipation-length parameter u_*^3/ϵ and ϵ is the dissipation rate.

Badri Narayanan & Ramjee (1969) attempted to meld these diverse observations into a unified structure by describing reverse transition in three consecutive states: (i) the disappearance of the turbulent bursts near the wall at $K_u \approx 3 \times 10^{-6}$; (ii) breakdown of the law of the wall at $K_p = 0{\cdot}02$; and (iii) the decay of turbulence intensity starting at $R_2 = 300$–400. While at first glance this description seems to accommodate all the observations reported above, stage (iii) strongly implies that the completion of laminarization is controlled by a critical value of R_2, whereas Launder & Jones (1969) suggested that K_u was the critical parameter. In summary, there still remain significant uncertainties not only in the precise values of the dimensionless parameters to employ as criteria, but also as to which parameter is the best to use in predicting the occurrence of laminarization.

The current study addresses a number of questions related to the above uncertainties. Does this flow demonstrate the same features as other accelerating turbulent flows? Can laminarization be predicted by the same parameters; is the order of magnitude the same; does any parameter provide a universal criterion or, if not, which is best? Is adequate modelling of this flow obtained with simple turbulence models? Part 2 further examines the correspondence between laminarization detection by mean measurements in this paper and by temporal burst measurements; also studied are the questions: (*a*) does the typical burst observed via the wall shear stress signal behave as the burst deduced from the fluctuating streamwise component (Blackwelder & Kaplan 1976); and (*b*) do these bursts scale on inner (wall) variables or outer (freestream) variables?

Section 2 outlines the numerical method used for the calculations, and §3 describes the apparatus and techniques. Experimental results, comparison with predictions and deduction of criteria related to laminarization are presented in §4 for nominally laminar conditions and in §5 for turbulent flows. Simple turbulence models for the near-wall region are also examined in §5, and §6 summarizes the conclusions of the first part of the study. More details and tabulated data are contained in the thesis by Murphy (1979).

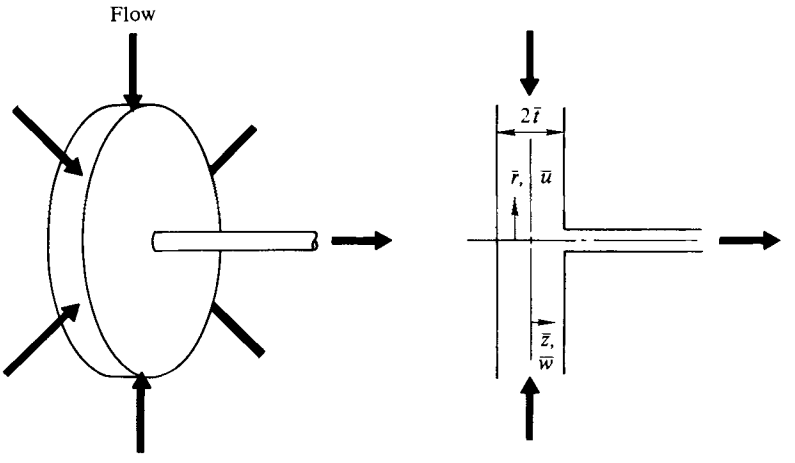

FIGURE 1. Idealized flow geometry.

2. Numerical method

The physical situation, shown in figure 1, consists of two stationary parallel circular disks separated by a distance $2\bar{t}$, with the origin for the transverse coordinate $\bar{z}$ located at the plane midway between the disks.† The radial coordinate and the transverse and radial components of velocity are denoted as $\bar{r}$, $\bar{w}$, $\bar{u}$ respectively. The fluid density and kinematic viscosity are $\bar{\rho}$ and $\bar{\nu}$ respectively. The analysis is restricted to primarily radial flow.

For steady incompressible flow of a viscous fluid with no azimuthal component of velocity (swirl), nor azimuthal variation of pressure or velocity, the governing equations consist of the continuity equation and two equations of motion written in cylindrical coordinates with appropriate boundary and initial conditions. In order to transform the governing equations into forms that have no free parameters except the turbulence model, we define the following dimensionless variables:

$$u = \frac{\bar{u}}{\bar{V}}, \quad w = \bar{w}\frac{R_0^{\frac{1}{2}}}{\bar{V}}, \quad r = \frac{\bar{r}}{\bar{t}R_0^{\frac{1}{2}}}, \quad z = \frac{\bar{z}}{\bar{t}}, \quad P = \frac{\bar{P}_i - \bar{P}}{\bar{\mu}\bar{Q}/4\pi\bar{t}^3},$$

where $\bar{V}$ is the bulk average velocity at any radius $\bar{V} = \bar{Q}/4\pi\bar{r}\bar{t}$, $\bar{Q}$ is volumetric flow rate, $R_0 = \bar{Q}/4\pi\bar{\nu}\bar{t}$ is an overall Reynolds number, and $\bar{P}$ and $\bar{P}_i$ are respectively the local and inlet values of the pressure. It should be noted that the overall Reynolds number is not a function of radius, and, since the non-dimensional radius is scaled inversely with $R_0^{\frac{1}{2}}$, small values of r can still correspond to substantial distances from the centre of the disks. For laminar flow viscous effects are of the same order as acceleration effects at $r = 1$ and viscous effects dominate when $r \gg 1$.

As a consequence of the above definitions, of the assumption that $R_0^{\frac{1}{2}} \gg 1$ and of an order-of-magnitude analysis (Murphy 1979), the governing equations for the three dependent variables can be reduced to the following:

continuity

$$\frac{\partial u}{\partial r} + \frac{\partial w}{\partial z} = 0,$$

† For convenience in §2 (and figure 3) only, we adopt the convention that dimensional variables are identified with an overbar while non-dimensional variables have none. In this paper all quantities are mean quantities unless specified otherwise.

radial momentum
$$u\frac{\partial u}{\partial r}-\frac{u^2}{r}+w\frac{\partial u}{\partial z}=r^2\frac{dP}{dr}+r\frac{\partial}{\partial z}\left(\frac{\bar{\nu}_{\text{eff}}}{\bar{\nu}}\frac{\partial u}{\partial z}\right),$$

and integral continuity
$$\int_0^1 u\,dz=1,$$

with the Reynolds shear stress represented in terms of an effective viscosity, $\bar{\nu}_{\text{eff}}=\bar{\nu}+\bar{\nu}_{\text{t}}$. These equations correspond to the usual boundary-layer approximations for internal flows. The momentum equation has full provision for the acceleration or inertial terms as well as the viscous term, and consequently the analysis is, in principle, applicable to flows ranging from slow viscous creeping flows to strongly accelerated flows. Boundary conditions are symmetry at the midplane and no slip at the impermeable wall. The inlet pressure can be specified as zero for reference. Entry radius r_{i} is chosen to correspond to the individual experiment, and the streamwise velocity is approximated as uniform at this position.

The van Driest (1956) mixing-length model

$$\bar{l}=\kappa\bar{y}[1-\exp(-y^+/A^+)],$$

and modifications thereof are employed to evaluate $\bar{\nu}_{\text{t}}$. The constant or damping factor A^+ is taken as 26 for the unmodified version and $\kappa=0{\cdot}4$ was used throughout. To treat growing and shrinking boundary layers within the duct, the mixing length is truncated at $\bar{l}=0{\cdot}09\bar{\delta}$. For laminar comparisons $\bar{\nu}_{\text{t}}$ is suppressed.

The momentum equation is parabolic, so an iterative marching technique (Bankston & McEligot 1970) developed for internal tube flows was extended (Murphy 1979). A finite-control-volume analysis is employed to generate a set of implicit finite-difference equations. These algebraic equations are solved successively and are then iterated to handle the nonlinearities in the convective terms in the momentum equation. The momentum equation and the integral continuity equation are solved simultaneously for $u(z)$ and P, and then the continuity equation is solved from the wall to the centreplane to obtain $w(z)$.

The solution accuracy was tested by successively refining the mesh to determine converged results for test cases. To conserve computer time, mesh parameters were then chosen to yield wall-friction results within about 1 % of converged values. Typically, fifty nodes in the z-direction were sufficient. However, at small r the boundary layer becomes quite thin, so 100 nodes were used and the nodes were distributed according to a power law in z so that the node spacing rapidly diminished as the wall was approached. In the radial direction the nodes were initially spaced by a dimensionless radius increment of 10^{-5}. This increment was allowed to increase by 10 % for each subsequent radial step until the radial spacing became equal to 0·01 times the dimensionless radius. Thereafter it was maintained at $0{\cdot}01r$.

3. The experiment

In order to examine which parameters dominated the flow behaviour, the apparatus was designed so that the acceleration parameters and local Reynolds number could be varied separately. Data were collected in equipment aimed at providing flows corresponding to the idealized situation pictured in figure 1. In general, room air entered the test section of parallel plates, flowed radially towards the exit, turned through a geometrical transition to a circular pipe and passed through a venturi flowmeter followed by flexible tubing before being exhausted by

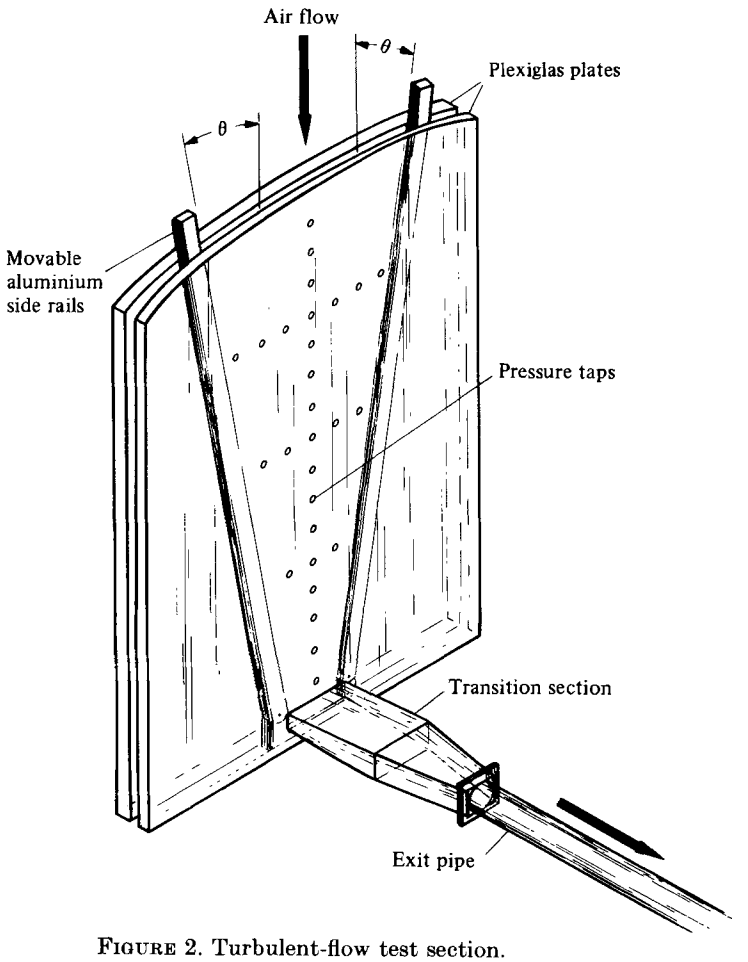

FIGURE 2. Turbulent-flow test section.

the blower which induced the flow. Flow rate was varied by adjustments to the blower. The test section and exit pipe were fabricated of Plexiglas to permit smoke-flow visualization. The current measurements concentrated on the surface shear stress, the pressure distribution and simple flow visualization, while profile measurements are deferred for a later study using larger dimensions and a different fluid.

Two test sections were employed: one circular as shown in figure 1 for laminar flow and a second one in the shape of a sector of a circle, as in figure 2, for turbulent and transitional flow. In the first, the plate spacing was varied from 0·92 mm (0·036 in.) to 51 mm (2 in.) to change the relation between K_u and the local Reynolds number, $Re = VD_h/\nu$, where D_h is the hydraulic diameter, twice the plate spacing. The effective entry was located at a radius of 0·29 m (11½ in.) and the air flowed inward to the exit hole, which was of 75 mm (3 in.) diameter. Plate edges were rounded to induce an approximately uniform flow at the inlet, corresponding to the initial condition imposed in the numerical predictions. The surfaces of these disks were smooth, with peak-to-peak flatness variations of 0·25 mm occurring with a wavelength of 50–100 mm. The effects of this variation were included in the uncertainty analysis.

For the turbulent-flow test section, the parallel plates were fixed at a spacing s of 12·7 mm (0·500 in.) and the sidewalls pivoted about the exit to vary the acceleration. With an exit width of 152 mm (6 in.) the cross-section was a rectangular channel with

a minimum aspect ratio of 12, thus providing a two-dimensional duct flow except in the vicinity of the sidewall boundary layers. The effective duct length was 1·14 m (45 in.), and each siderail could be moved a maximum of 20° from the vertical. In this radial geometry the effective radius at the outlet, measured from a virtual origin where the siderails would have intersected, was $0{\cdot}152/2 \sin\theta$ m. The inlet was formed with sharp 90° corners, which, in conjunction with the shear layer in the induced vena contracta, were intended as 'trips' so that the transition to turbulent flow would occur as soon as possible and not be impeded as by a smooth nozzle-shaped inlet. One plate contained a centreline port for the surface stress sensor or for insertion of probes into the flow, while the other was instrumented with an array of taps to measure the static pressure distribution. The plate with the surface sensor was planed on a horizontal mill to a waviness of less than 50 μm.

Pressure taps consisted of 0·7 mm (0·027 in.) holes drilled 3 mm deep from the inside face to avoid burrs on the test surface. The small hole diameter was chosen to ensure that the pressure tap geometry would not affect the measured pressures (Shaw 1960). The taps were then completed by drilling larger holes connecting from the outside and were connected via a manifold to the transducer of an MKS Baratron capacitance manometer. Transducers with ranges of 1 mmHg and 100 mmHg were used as appropriate. Both were calibrated at ten pressure difference levels at the manufacturer's facilities; the maximum discrepancy from the indicated reading was 0·06 %.

The absolute atmospheric pressure was measured with a mercury barometer with resolution of 0·1 mmHg. Inlet air temperature, required to determine the air viscosity and density, was measured with a Thermo-Schneider mercury thermometer graduated in 0·2 °C increments. Smoke was injected manually with a 'smoke gun' utilizing the reaction between titanium tetrachloride and water vapour in the air. Several positions at the periphery were chosen to check visually that the flow was truly radial without swirl and laminar or turbulent as appropriate. Pressure difference measurements between two taps at the same radius also demonstrated a high degree of azimuthal symmetry.

The venturi flowmeter was manufactured commercially with pressure taps upstream and at the throat. Honeycomb was placed downstream of the venturi to inhibit propagation of swirl components induced by the outlet blower; smoke-flow visualization confirmed its success. The discharge coefficient was evaluated as a function of the Reynolds number by calibrating with a bell prover at the flow-calibration facility of the Sandia Laboratories in Albuquerque and with a laminar flow element at the University of Arizona.

Surface shear stresses were measured with a flush-mounted Model 1237 hot-film sensor manufactured by TSI and installed on removable ports. The heated platinum film was 1 mm (0·040 in.) wide in the lateral direction and 0·12 mm (0·005 in.) long in the streamwise direction. These ports were flush to within 10 μm, and the probe bodies on which the sensors were mounted were flush to within 5 μm, or a maximum of 1·5 viscous units in the worst case; for comparison, Bellhouse & Schultz (1966) found that purposely introducing mismatches of 75 μm did not affect shear-stress measurements in turbulent boundary layers. The sensor was calibrated in place and was not disturbed for any of the measurements reported here. The probe was operated at a constant resistance corresponding to a spatial average temperature of 250 °C by a TSI 1050 anemometer system with bridge voltage measured by a Fluke 8300A digital voltmeter.

Since the sensor is heated resistively by an electrical current, the quasi-steady thermal boundary condition is ideally a constant wall heat flux. The appropriate

Lévêque solution for this situation is given by Worsoe-Schmidt (1967) and leads, as a first approximation, to the relation

$$\frac{e^2 - e_0^2}{R_e} = A\,\tau_w^{\frac{1}{3}},$$

where e is the voltage and R_e is the electrical resistance of the filament. Following Bellhouse & Schultz (1966) the quantity e_0^2 is used to represent other heat losses. The constants A and e_0^2 were determined by *in situ* calibration, operating the test section as a rectangular duct of constant cross-section so the flow was fully developed at the sensor; the shear stress could then be determined from the measured pressure gradient via a force balance with the assumption of uniform shear stress over the duct circumference. The sensor was calibrated over a range of three decades in shear stress, and therefore pressure gradient, and satisfied the $\tau_w^{\frac{1}{3}}$ dependence upon e^2 from about 0·03–4 Pa.

Brown (1967) deduced that the idealizations of a first-order Lévêque solution would be valid provided that the non-dimensional length in the streamwise direction is less than about $64Pr$, or $l^+ \lesssim 45$ for air. In the present study the maximum effective value of l^+ was estimated to be between 12 and 25. As Blackwelder & Kovasznay (1972) and others have observed, the viscous layer thickens in favourable pressure gradients so this criterion would be conservative in this experiment.

The frequency response of the sensor was estimated in air with the electronic square-wave method (Freymuth 1977). The cutoff frequency was found to be 30 kHz, whereas the predominant frequency of the turbulent fluctuations was only 1 kHz or less; there was some evidence of frequencies to about 5 or 10 kHz, but they carried very little energy. The temporal procedures and measurements are reported in part 2.

Experimental uncertainties have been estimated in the manner of Kline & McClintock (1953). They have been indicated by brackets on the figures presenting results. For the comparison of measurements with predictions the uncertainties can be of two types: direct and associated. Direct uncertainties are those relating to the measurement and quantities deduced from it, e.g. an uncertainty in a pressure difference or in a non-dimensional pressure defect. Associated uncertainties enter the comparison indirectly via the prediction. The comparisons are conducted using measured quantities, such as flow rates, to determine the initial conditions for the predictions; therefore there is an induced uncertainty in the predicted results. Rather than present these induced uncertainties in the form of a family of predicted curves, they have been transformed to associated or equivalent uncertainties in the data plotted. Thus the brackets represent the uncertainty associated with the predictions when appropriate.

4. Laminar-flow results

A total of 15 experiments were conducted with laminar flow in the circular-disk apparatus to test the validity of the experimental procedures. In this situation the effective viscosity is unambiguous, so the comparison serves as a confidence test for the experiment. In addition, the results provide evidence of dominance of the acceleration parameter, rather than local Reynolds number, in determining the flow regime in this configuration.

A large variation of parameters was desired and was attained. Flow rates were varied over an order of magnitude and spacings ranged almost two orders of

magnitude. As a result, the Reynolds number varied from 210 to $2{\cdot}1 \times 10^4$, the dimensionless inlet radius r_i ranged from 0·17 to 3·35 and K_V fell between $9{\cdot}5 \times 10^{-6}$ and $2{\cdot}2 \times 10^{-4}$. The lateral strain-rate ratio, as defined by Smits *et al.* (1979), is of order $(V/r)/(V/\frac{1}{2}s)$ or $s/2r$ and is negative. For this set of experiments this ratio ranges from about $-0{\cdot}01$ to $-0{\cdot}17$ at half-radius.

All experiments were conducted at room temperature, approximately 25 °C, and the pressure drop in the test section was less than 5 mmHg. Inlet pressure was close to the atmospheric pressure of about 620 mmHg (elevation $\approx 2{\cdot}1$ km m.s.l.) so the air could be considered non-compressed to correspond with the constant-density idealization of the numerical predictions. The most important experimental uncertainties were those related to flow rate, spacing (e.g. surface waviness at close spacings) and slight fluctuations in the room pressure ($\pm 0{\cdot}001$ mmHg) at large spacings.

Details of numerical predictions for laminar flow are presented by Murphy (1979). For comparison with measurements, calculations were conducted with a uniform initial velocity profile assumed to exist at the radius where the outermost pressure tap was located. This inlet velocity was determined from the measured flow rate with air properties evaluated at the measured room temperature and pressure. For most runs the dimensionless inlet radii were less than one, so these flows never attained the parabolic velocity profile of large r but instead were continuously developing. Since the numerical solutions are based on the governing equations for developing internal boundary layers, the predictions are still applicable.

Predictions are compared to the measurements of streamwise pressure distribution for four typical runs in figure 3. Flow is from right to left, i.e. converging from larger to smaller radii. Dimensionless inlet radii range from 0·3 to almost 2, spanning almost the full range of the experimental investigation. The magnitudes of the radii are such that both acceleration and viscous effects were important, so that asymptotic relationships for $r \gg 1$ and $r \ll 1$ cannot be used. Calculations for alternative entry profiles have shown that the predicted results approach a single, continuously developing solution beyond the entry region. This behaviour is evident in both the analytical results and measurements shown on figure 3. Agreement between the data and the predicted pressure drop is seen to be generally close and well within the estimated experimental uncertainties, thereby implying that these estimated uncertainties are conservative.

The experiments agreed well with the laminar analyses for local Reynolds numbers from 210 to 20700. The agreement at low Reynolds numbers, where one would expect the flows to be laminar, whether accelerated or not, serves to establish the validity of the experimental procedures and measurements. Further, it appears that, based on this agreement, all these flows were predominantly laminar up to local Reynolds numbers of 20700. Secondary evidence that these flows were laminar and radial was provided by viewing the smoke pathlines from three directions; no rapid mixing or diffusion was visible. No attempts were made to inhibit laminar-to-turbulent transition; residual turbulence in the entering air was not eliminated by screens, and the surface smoothness was only that of commercial Plexiglas. Consequently these experimental conditions were actually favourable for laminar-to-turbulent transition had this transition not been suppressed by acceleration. Thus it appears that, for the range of parameters of this experiment, the induced acceleration dominated over the local Reynolds number in determining the flow regime. This observation was to be expected, but it still warranted confirmation.

As noted in §1, a number of authors have recommended critical values of the

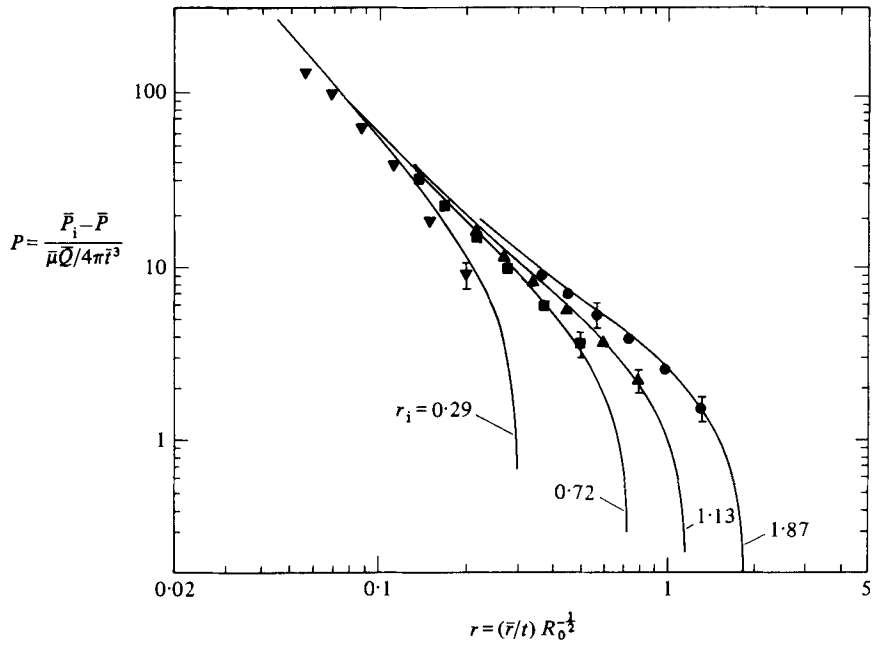

FIGURE 3. Overall comparison of measured and predicted pressures in laminar flow: ●, local-Reynolds-number range 210–1080; ▲, 570–2930; ■, 1430–7300; ▼, 1060–5440; ——, laminar prediction.

acceleration parameters K_V, K_p and K_τ above which a turbulent boundary layer can be expected to revert to a laminar one. Although this conclusion was derived from experiments in which the flow was still intermittently turbulent, it is reasonable to expect that if a flow is initially laminar and the critical value is exceeded, then the flow will remain laminar – unless there is a substantial change in the behaviour due to changes in geometry. In the present study, deduced values of K_V, K_p and K_τ were well above their suggested critical values, and the flow apparently remained laminar, so the experimental results are consistent with the laminarization criteria proposed for other geometries. Further evaluation of these criteria resulted from data obtained with the second flow apparatus, discussed next.

5. Turbulent flow

The purpose of the measurements in the sector-shaped test section was to examine a wide range of turbulent flows that were converging laterally and to study the variation over the range from fully turbulent to near-laminar flow. Mean wall parameters are presented here, and the transient signals are analysed in part 2.

Since no flow-development region was present ahead of the test section, the flow from the room was essentially laminar at the entry but was strongly disturbed by the sharp edges and the shear layer at the resulting vena contracta. With lateral convergence the flow then accelerated continuously to the exit. As a consequence of their definitions, the local Reynolds number increases as r decreases ($Re \propto 1/r$) while the acceleration parameter K_V remains constant. In contrast with many laminarization experiments with short test sections (Narasimha & Sreenivasan 1973), the induced acceleration extended over 80 channel spacings in the present experiment.

Thirty-four experiments, in which pressures and mean shear stresses were measured, were completed with the apparatus shown in figure 2, and an additional 27

experiments were conducted with temporal measurements of wall shear stress, leading to the results of part 2. Flow rates, overall Reynolds numbers, wall shear stresses and pressure drops varied by almost three orders of magnitude. Dimensionless radii were kept in the range of about 0·1–1 so that acceleration would not overwhelm viscous effects. It should be recalled that for laminar flows the two effects are roughly equal for $r = 1$. For turbulent flows $\nu_{\text{eff}} \gg \nu$, so that viscous effects were even more important. Convergent flow angles were adjusted to vary the acceleration at a given flow rate. The ranges of parameters examined in the converging channel were local Reynolds numbers from 1600 to 68000, acceleration parameters $K_V = 1/R_0$ from $2{\cdot}6 \times 10^{-8}$ to $1{\cdot}1 \times 10^{-5}$ and convergent half-angles from $\frac{1}{4}°$ to 16°. The lateral strain-rate ratio ranged from about $-0{\cdot}0003$ to $-0{\cdot}006$ for minimum to maximum convergent half-angles respectively.

Again entering conditions were room pressure and temperature. A check of the transverse taps revealed no lateral dependence of pressure at any of the streamwise positions where these additional taps were located. The overall pressure-drop uncertainty (direct plus associated) was dominated by the uncertainties in flow rate and channel spacing. The uncertainty in wall shear stress due to probe voltage measurement was derived from repeatability studies. Despite measurement of the mean-shear-stress signals with a precise Fluke 8300A integrating digital voltmeter, the sensitive relationship between τ_w and $e^2 - e_0^2$ led to the sensor-voltage uncertainty dominating the overall shear-stress uncertainties, along with the flow-rate uncertainty. The shear-stress uncertainties increase with half-angle and with decreasing flow rate.

5.1. *Straight rectangular duct*

Preliminary measurements were conducted with parallel siderails to form a rectangular duct with constant cross section and an aspect ratio of 12. These experiments mainly validated the apparatus, served as a convenient method of calibrating shear-stress probes *in situ*, and provided a reference for comparison with the entry behaviour in the accelerated flows. Hartnett, Koh & McComas (1962) found that when the aspect ratio was 5 or 10 in a fully developed flow the peripherally averaged wall shear stress was about 4% higher than the Blasius correlation for the range $6000 < Re < 10^5$. With the abrupt entry to the present test section, the streamwise pressure gradient was constant after $x/s = 20$. The friction factors $f = 2\tau_w/\rho V^2$ of the present paper agree with the Blasius correlation to within 4% for $Re > 10^4$, but diverge slightly at lower Reynolds numbers. The measurements for fully developed laminar flow yielded $fRe \approx 21{\cdot}1$, in reasonable agreement with the numerical prediction of $fRe \approx 21{\cdot}8$ by Kays and Clark (see Kays & Crawford 1980) for an aspect ratio of 12.

Two-dimensional numerical predictions with the van Driest model yielded friction factors that are 5–10% higher than the Blasius correlation and the data from the rectangular duct for $Re > 10^4$. As the Reynolds number was lowered, the numerical prediction disagreed slightly further towards higher values. Since the numerical method was next employed for comparison to the data for laterally converging duct flow, it is appropriate to recognize that, for both laminar and turbulent flow, the two-dimensional idealization can be expected to overpredict pressure gradients and wall shear stresses slightly.

5.2. *Streamwise pressure distribution*

The primary new data are the measurements of flow in the laterally converging duct. Figure 4 presents typical results for a range from slight to maximum lateral

convergence. Flow is again from right to left. Shown also are the two-dimensional numerical predictions using both the van Driest model and purely laminar flow. The data are referenced to the pressure at $x/s = 8$, and the predictions are based on an initial condition of a uniform velocity at the actual entrance, $x = 0$. The coordinate r still measures radial distance from the virtual centre, but x measures the downstream distance from the entry. Each prediction is based on the measured flow rate for the run.

Figure 4(*a*) is for a high entering Reynolds number and a minimal convergence, a half-angle of $\frac{1}{4}°$ with dimensionless radius decreasing from 0·475 at the entry to 0·445 at the exit. In light of the comments above regarding rectangular ducts versus pure two-dimensionality, it appears that it represents a normal, quasi-developed, fully turbulent flow, as would be expected from evaluation of any of the laminarization criteria in §1.

On the other hand, a different situation appears in figure 4(*b*) with a slight convergence angle and a lower Reynolds number; the lateral strain rate ratio is about $-0{\cdot}002$ at the location of the shear-stress sensor in this case. The pressure difference is significantly less than for the fully turbulent prediction, but is still well above that for laminar flow, implying some turbulent momentum transport. As indicated in part 2, wall shear-stress signals for comparable conditions show substantial fluctuations, with no obvious difference from an unaccelerated flow at the same Reynolds number. Nevertheless, for this slight convergence and strain rate there is an observable effect on the pressure distribution.

As the flow proceeds downstream there appears to be no tendency to approach either prediction; this situation is considered to correspond to the laminarescent state suggested by Kline (1967). Since the pressure drop is an integral parameter from the reference position to the location x, it is difficult to discern from this figure whether the local data downstream are representative of laminar or turbulent behaviour. This issue will be examined further in §5.3, presenting direct comparisons between pressure-gradient data and their predictions.

The most extreme case is shown in figure 4(*c*). With the minimum flow rate and maximum lateral convergence in the range of data, the acceleration parameter is $1{\cdot}1 \times 10^{-5}$. The component of pressure drop due to acceleration is so large relative to the viscous component that, compared with figures 4(*a*, *b*), there is little difference between the laminar and turbulent predictions. The local Reynolds number in figure 4(*c*) is 1200 at the entry, increases to 3300 at the wall sensor and is 8150 at the exit. The measured pressure distribution agrees with the laminar prediction until $x/s \approx 50$ ($Re \approx 3000$). The result is not surprising since acceleration is known to increase critical Reynolds numbers and may inhibit the development of fully turbulent flow even if transition begins.

The behaviour of all runs with convergence half-angles from $\frac{1}{4}°$ to 8° is summarized by figure 5, where a comparison parameter ϕ_p is plotted versus the acceleration parameter K_V. The parameter ϕ_p can be considered to be an indicator of whether the pressure distribution (after the vena contracta) in this length of the test section corresponds to laminar flow, to fully turbulent flow as predicted by a van Driest model or to an intermediate condition; its definition is

$$\phi_p = \frac{\Delta p_{\text{meas}} - \Delta p_{\text{lam}}}{\Delta p_{\text{turb}} - \Delta p_{\text{lam}}}.$$

The pressure drop Δp is evaluated from the first useful pressure tap, at $x/s = 8$, to the pressure tap at $x/s = 56$, nearest the shear-stress sensor. A value of ϕ_p equal to

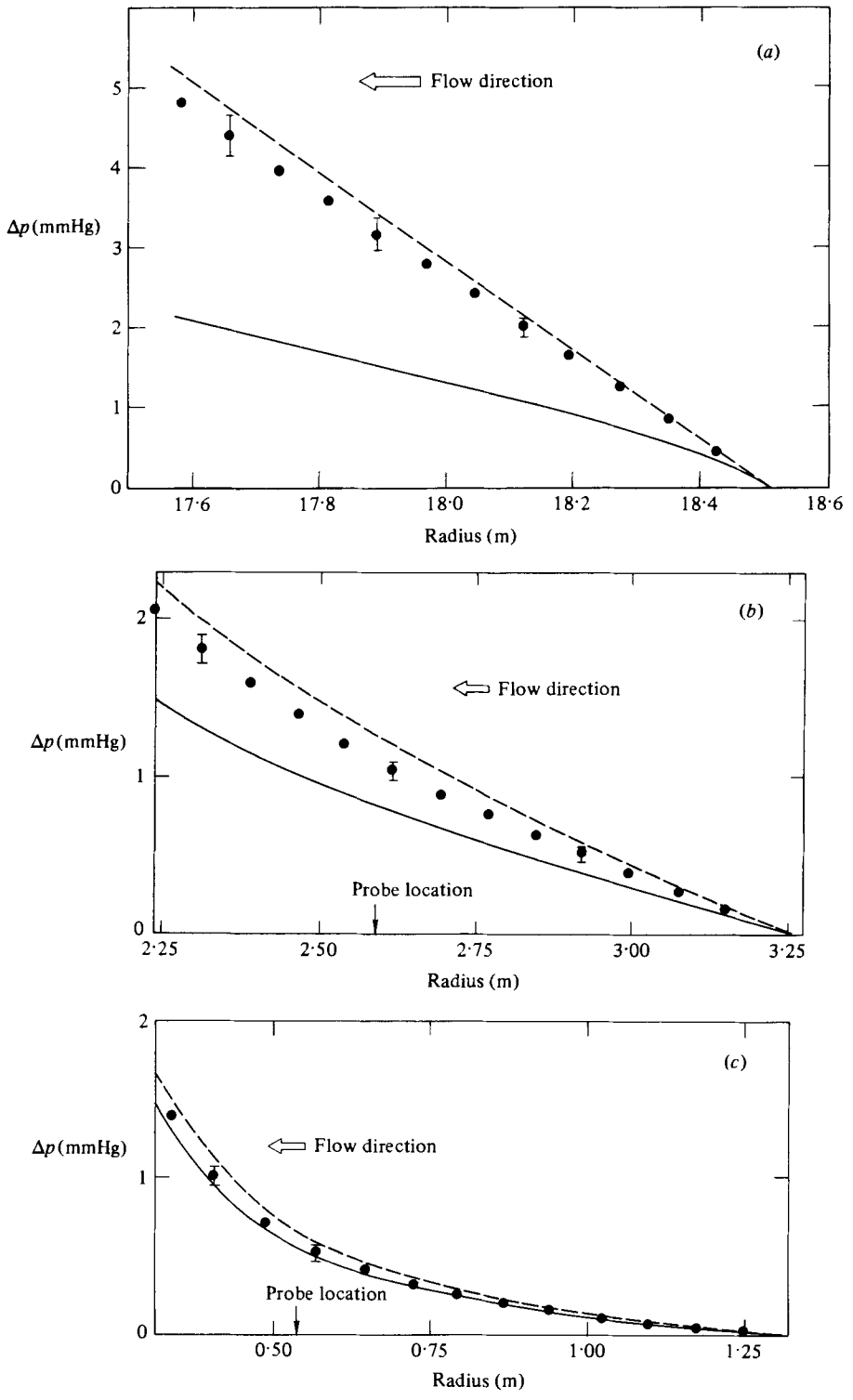

FIGURE 4. Measured and predicted pressure distributions: (*a*) $\theta = \frac{1}{4}°$, $K_V = 2{\cdot}61 \times 10^{-8}$, $Re_{\text{probe}} = 52400$, $Re_{\text{entry}} = 50320$; (*b*) $\theta = 2°$, $K_V = 3{\cdot}95 \times 10^{-7}$, $Re_{\text{probe}} = 24900$, $Re_{\text{entry}} = 19600$; (*c*) $\theta = 16°$, $K_V = 1{\cdot}11 \times 10^{-5}$, $Re_{\text{probe}} = 3300$, $Re_{\text{entry}} = 1200$. ——, laminar prediction; – – –, turbulent prediction (van Driest model).

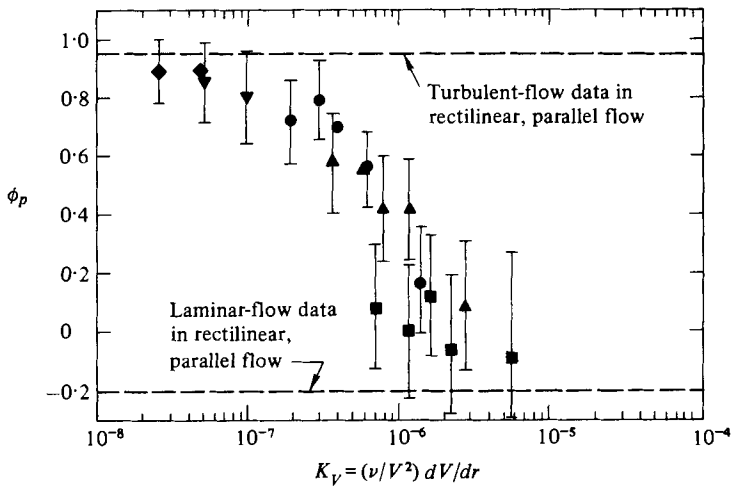

FIGURE 5. Apparent laminarization of terms of initial pressure drop and K_V: ◆, $\theta = \frac{1}{4}°$; ▼, $\frac{1}{2}°$; ●, 2°; ▲, 4°; ■, 8°.

zero corresponds to agreement with the two-dimensional laminar prediction. Unity represents agreement with predictions from a van Driest turbulence model, again for two-dimensional flow.

By covering a range of convergence angles, the local Reynolds number is also varied at a given value of K_V. The general trend of a decrease in ϕ_p as K_V increases appears to be independent of convergence angle. For $K_V \lesssim 10^{-7}$ the data agree with the turbulent prediction – thereby implying that the van Driest model is valid for estimating pressure drop, and presumably heat and mass transfer, for that range. For $K_V \gtrsim 4 \times 10^{-6}$ the implication is that a laminar idealization is adequate for $x/s \gtrsim 56$. In the range $10^{-7} \lesssim K_V \lesssim 4 \times 10^{-6}$ there is an indication of significant turbulent transport before $x/s = 56$, but the turbulence model must be improved to account for it.

Narasimha & Sreenivasan (1979) have adopted the pragmatic definition that a flow is relaminarized if its development can be understood without recourse to any model for turbulent shear flow; thus fluctuations need not have vanished but their contribution to mean-flow dynamics is negligible. In this sense the runs at $K_V \gtrsim 4 \times 10^{-6}$ could be considered laminarized, as will be seen later, but a better description would probably be that they remain laminar since it appears likely that the flow was laminar throughout, rather than being turbulent at some point and subsequently laminarized.

5.3. *Local pressure gradients downstream*

The local behaviour can be examined better by studying the variation of the pressure gradient and the mean wall shear stress. Typical data for a range of K_p are compared to predictions in figure 6; the data points presented are calculated by taking the difference between pressure measurements at adjacent taps. All runs shown have local Reynolds numbers of the order of 2×10^4 at the location of the wall sensor, except the last one, which demonstrates the situation with a high acceleration parameter. Figures 6(*a*, *b*) correspond respectively to figures 4(*a*, *b*).

For most runs the pressure gradient from $x/s = 2$ to $x/s = 8$ is small, as expansion from the vena contracta near the entry counteracts the wall friction. At low K_V it becomes approximately constant after $x/s \approx 15$–30, as in a duct of constant

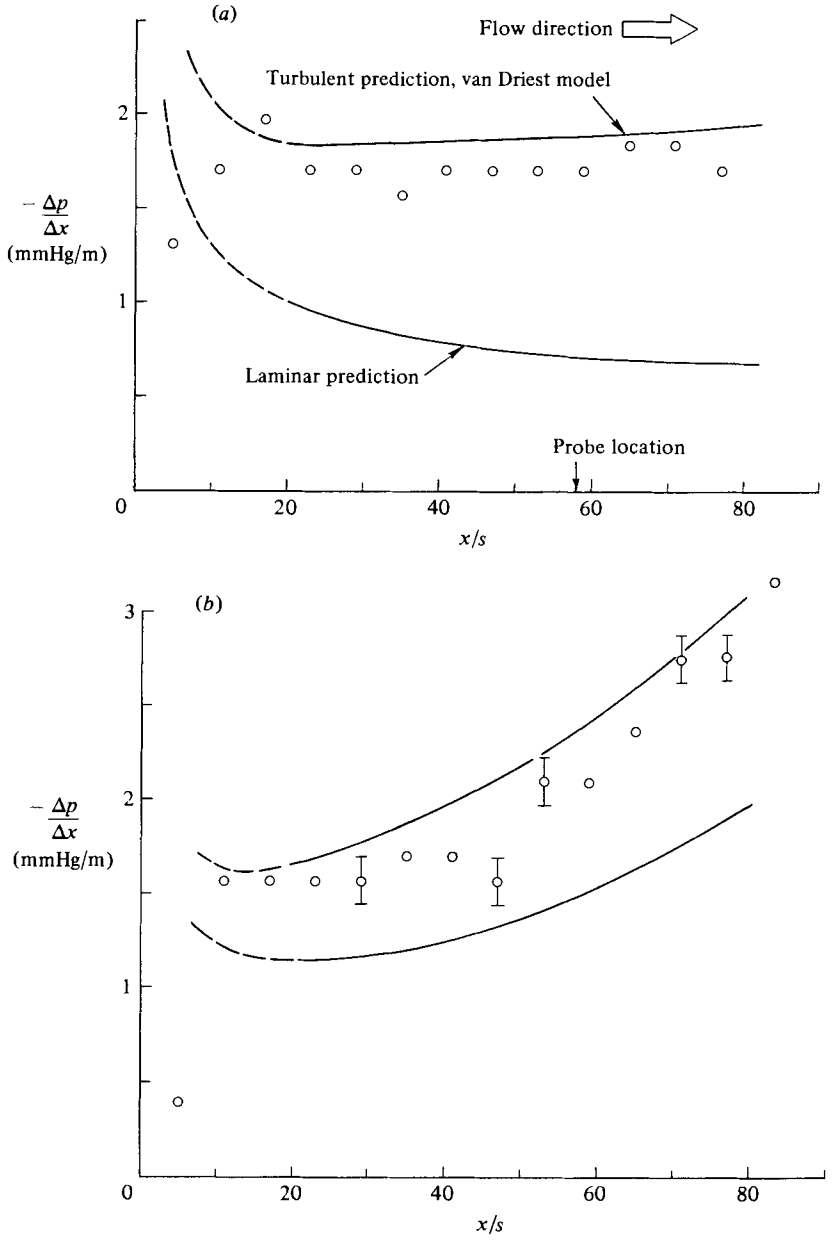

FIGURE 6(*a*, *b*). For caption see facing page.

cross-section. Near the exit of the test section dp/dx begins to increase slightly owing to slight acceleration. As K_V is increased, the length of the region with constant dp/dx (or the apparently fully developed region) becomes shorter as the bulk acceleration becomes more important, so that dp/dx becomes larger in the exit region. At high K_V the constant region disappears as this exit region extends forward to overlap the usual entry. Finally, in runs at the largest values of K_V, dp/dx increases continuously from entrance to exit as the pressure gradient due to acceleration dominates.

Because $x/s \approx 20$ is a location where the choice of inlet condition – uniform entry as in analyses or sharp-edged as in the experiment – appears unimportant, the

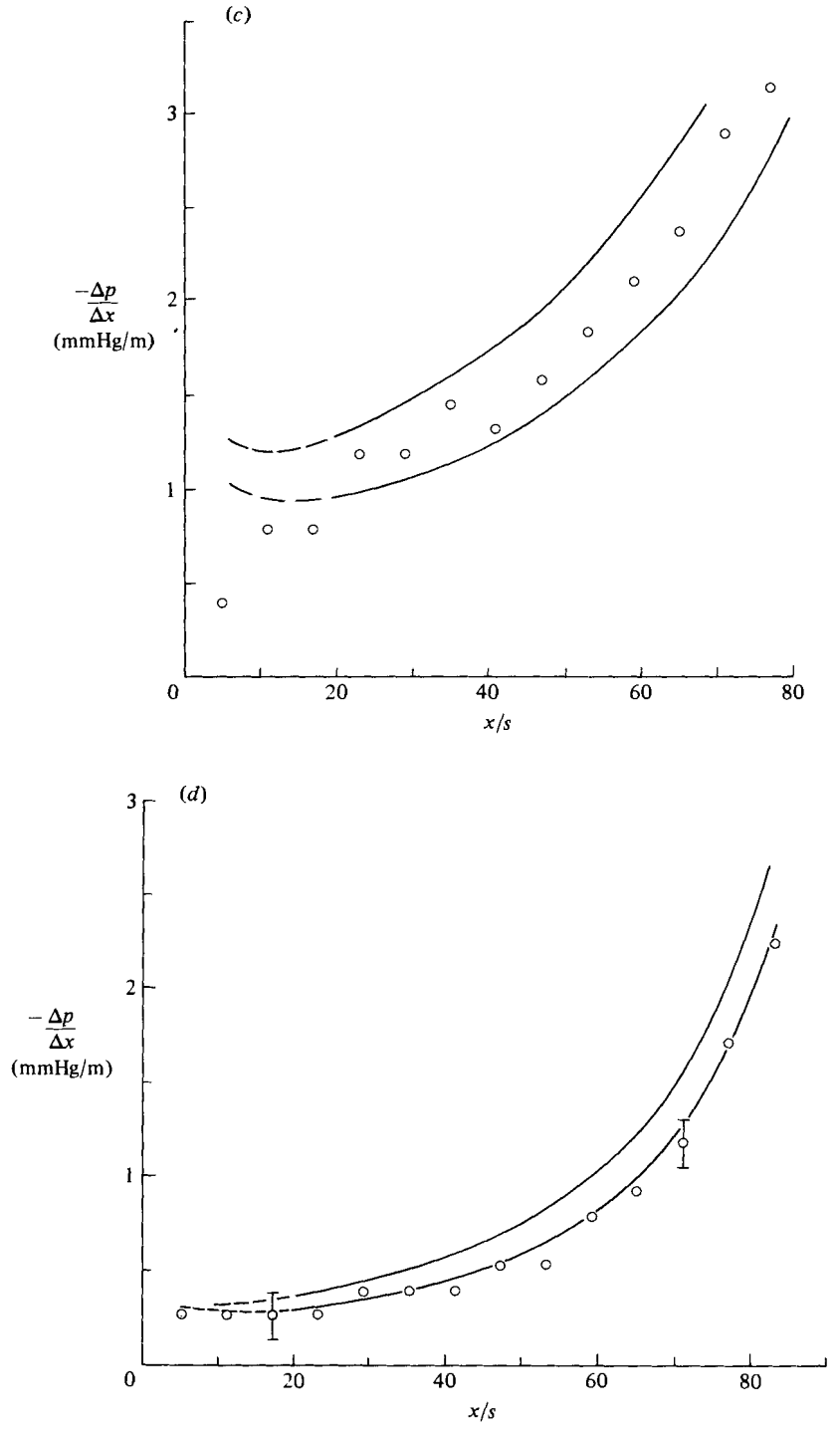

FIGURE 6. Measured and predicted pressure gradients: (*a*) $\theta = \frac{1}{4}°$, $K_V \approx 4{\cdot}9 \times 10^{-8}$, $Re_{\text{entry}} \approx 27\,500$, $Re_{\text{probe}} \approx 28\,200$; (*b*) 2°, 4×10^{-7}, 19400, 24900; (*c*) 4°, $7{\cdot}8 \times 10^{-7}$, 14400, 21600; (*d*) 8°, $2{\cdot}3 \times 10^{-6}$, 6400, 11300.

numerical predictions are plotted as solid curves from $x/s = 20$ to the exit in figure 6. In each part of the figure the upper curve represents the van Driest model and the lower is for laminar flow. The dashed lines demonstrate the entry region that would be predicted if the initial profile were uniform at $x = 0$ as for a bell-mouthed entry. As the convergence angle increases, the acceleration parameter K_V increases, the rate of increase of dp/dx increases near the exit and the percentage difference between the two predictions decreases.

In figure 6(*a*) it is seen that at the convergence angle of $\frac{1}{4}°$ the data agree approximately with the turbulent prediction for $x/s \gtrsim 20$; the measurements are slightly lower, as expected from the preliminary experiments in the straight duct.

At $\theta = 2°$ and $K_V \approx 4 \times 10^{-7}$ there is already a significant effect of acceleration on the local pressure gradient. However, it is not clear whether there is any effect on turbulent transport of momentum. Again the measurements show approximate agreement with the turbulent prediction but are slightly lower on average than in the previous figure. The vertical brackets in the figure demonstrate the limit of resolution of $\Delta p/\Delta x$ caused by the pressure-drop instrumentation in this run; these limitations decrease when integrating the pressure drop over a greater distance as in figure 4.

An apparent reduction in turbulent transport is evident in figure 6(*c*) for $\theta = 4°$ and $K_V \approx 7{\cdot}8 \times 10^{-7}$. By $x/s \approx 20$ the local measurements fall to a level intermediate between the two predictions, 'laminarescent' in the Kline (1967) terminology, and then remain there to the exit.

Figure 6(*d*) shows that the results for $K_V \approx 2{\cdot}3 \times 10^{-6}$ agree with the laminar prediction to the exit. By the definition of Narasimha & Sreenivasan (1979) this run would be considered laminarized in the range $60 \lesssim x/s \lesssim 80$ (where the local values of $\Delta p/\Delta x$ have adequate resolution).

The casual observer might consider the small difference between the two predictions in figure 6(*d*) as an indication that the question of whether laminar or turbulent flow occurs is unimportant at these conditions. However, near $x/s = 80$ there is still a difference of more than a factor of two between the predicted friction factors. Thus, there would still be significant differences in heat transfer, mass transfer, fouling and erosion depending on whether the flow were turbulent, laminar or intermediate.

In general, examination of local pressure gradients confirmed the conclusions suggested from the integral comparisons ϕ_p. If one were to define a local comparison parameter based on dp/dx, say $\phi_{dp}(x)$, it would appear to be approximately self-preserving from $x/s = 20$ to the exit.

5.4. *Local wall shear stress downstream*

The wall sensor also provides a means to quantify the apparent flow regime locally. In part 2 the effect on bursting is examined; here the mean wall shear stress at the location of the sensor is compared with numerical predictions for the same location.

A local comparison parameter can be defined, in a manner analogous to ϕ_p, as

$$\phi_\tau = \frac{\tau_{\mathrm{w\,meas}} - \tau_{\mathrm{w\,lam}}}{\tau_{\mathrm{w\,turb}} - \tau_{\mathrm{w\,lam}}}.$$

Again zero corresponds to laminar flow and unity to a fully turbulent approximation, both two-dimensional.

Use of ϕ_τ permits investigation of questions concerning proposed laminarization parameters and criteria. The parameters

$$K_p = (\nu/\rho u_*^3)\, dp/dx \quad \text{and} \quad K_\tau = (\nu/\rho u_*^3)\, (\partial\tau/\partial z)_{\mathrm{w}}$$

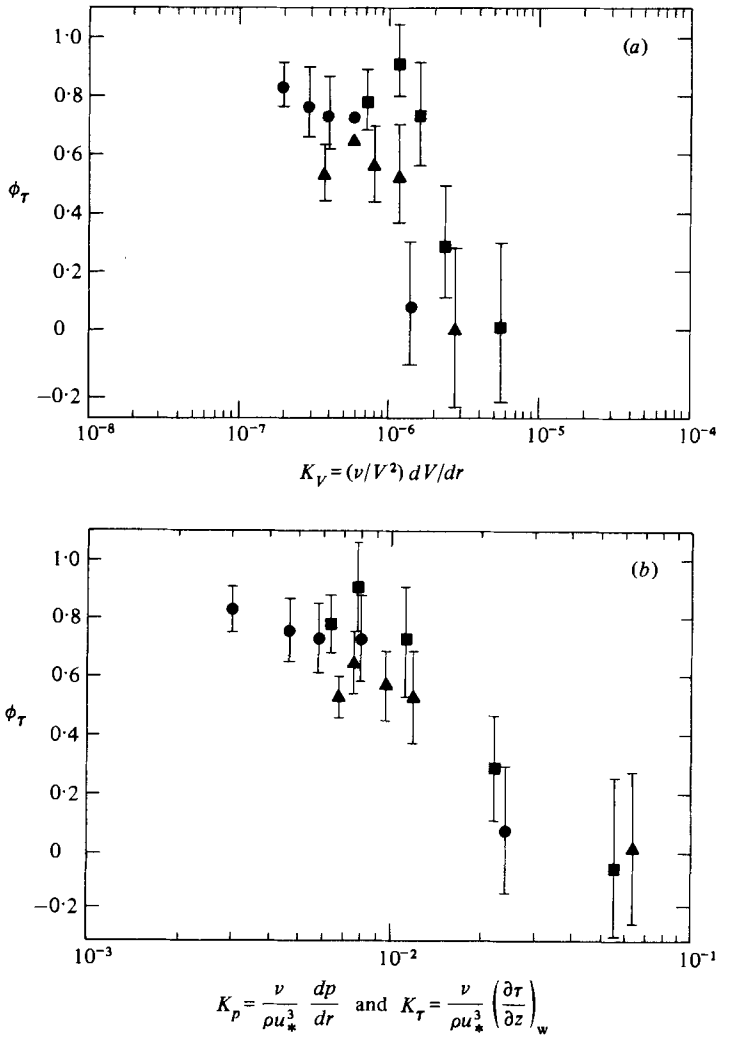

FIGURE 7. Apparent laminarization: (*a*) in terms of local shear stress and K_V; (*b*) in terms of local shear stress and K_p or K_T. ●, $\theta = 2°$; ▲, 4°; ■, 8°.

cannot readily be evaluated for an interval – and it is not clear that they would be meaningful if they were. With pointwise evaluation this difficulty does not arise.

The comparisons in figure 7 show that ϕ_T follows the same general trend with both acceleration parameters, i.e. a decrease as the acceleration parameter is increased. For $K_V \gtrsim 2 \times 10^{-7}$, ϕ_T shows some reduction from the fully turbulent result while the data are near the laminar predictions for $K_V \gtrsim 2 \times 10^{-6}$. The data for ϕ_T (K_p) correlate better than ϕ_T (K_v); this observation suggests that K_p may be the preferable criterion, but the improvement is not sufficient to be definitive. Divergence from fully turbulent results begins near $K_T = K_p = 0{\cdot}003$ and laminar values are approached in the vicinity of $K_T = K_p = 0{\cdot}04$ approximately. The lower extreme for K_T is consistent with the choice of a 'critical' value by Narasimha & Sreenivasan (1973), whereas the higher limit for K_p is of the same order, but twice this 'critical' value for pipe flow suggested to Patel & Head (1968). However, the technique of Patel & Head would tend to determine a threshold situation rather than more-complete

laminarization. At both extremes the approach to the limiting prediction is gradual as K is varied; there does not appear to be an abrupt threshold behaviour. Between the limits turbulent-transport processes are reduced but not eliminated.

As noted by Narasimha & Sreenivasan (1979), different workers have used different methods for recognizing the onset of relaminarization from a turbulent boundary layer and different parameters as criteria for the occurrence of reversion to a quasi-laminar state. As demonstrated in their table 1 some investigators examine phenomena identifying the former (not fully turbulent) while others measure the latter (near-laminar) directly or indirectly. Criteria based on recognizing onset, such as departure from a wall law (Patel & Head 1968) or from normal turbulent boundary-layer characteristics (Launder & Stinchcombe 1967), correspond to the present examination for $\phi < 1$. Those relating to cessation of bursting (Schraub *et al.* 1967) or agreement with a quasi-laminar limit (Narasimha & Sreenivasan 1973) correspond approximately to ϕ approaching zero. Studied in these terms there is general agreement between the present laterally converging entry flow and studies of accelerating flows in other geometries.

It is important to note that the present study does not claim to measure the completed process as it might occur for a flow that was initially 'fully turbulent'. Unlike some experimental apparatus, in which an entry section of constant cross-section is provided to establish fully developed turbulent flow prior to entering the acceleration section, we elected to accelerate the flow immediately upon entry, so as to have an acceleration length as long as possible and to ensure that the turbulent characteristics had ample time and distance to adjust to the acceleration. As a consequence of this immediate acceleration it is probable that the flow near the entrance experienced at least partial laminarization. Despite this limitation, we believe the results are indicative of the state to which accelerated flows would eventually evolve. That is, even if an experiment were to have a constant-area entry section, the 'history' of this fully developed turbulence would eventually be lost and the asymptotic nature of the turbulence would depend on the acceleration only, not upon the details of the entry section. It is this asymptotic state that we believe was measured.

If the definition of laminarization by Narasimha & Sreenivasan (1979) is adopted, ϕ_τ can be considered as a local measure of laminarization. With ϕ_p an integral measurement over the distance from the entrance, a run that underwent a retarded transition to a fully turbulent behaviour before $x/s = 56$ would appear as a partially laminarized run; however, in terms of ϕ_τ it would be calculated as a turbulent run if its wall shear stress had reached an equilibrium turbulent state prior to the sensor at $x/s = 58$. Thus use of ϕ_τ eliminates some 'history effects' in the comparisons. The similarity of the ϕ_τ and ϕ_p results in figures 5 and 7 (*a*) leads us to conclude that the flow was indeed laminarescent nearly from the entrance, and that little change occurred from that point to $x/s = 58$.

Departure of ϕ_τ from unity near $K_\tau = 0{\cdot}002$–$0{\cdot}004$ agrees with departure of wall-layer flow from a modified wall law for $K_p \gtrsim 0{\cdot}004$ (Patel & Head 1968, as corrected by Narasimha & Sreenivasan 1973). Likewise, the approach to $\phi = 0$ at $K_V \approx 2 \times 10^{-6}$–$4 \times 10^{-6}$ provides a criterion of the same order of magnitude as apparent cessation of bursting in the wall region at $K_V \gtrsim 3{\cdot}5 \times 10^{-6}$ (Schraub *et al.* 1967); measurements of bursting phenomena obtained in the present investigation are reported in part 2.

5.5. *Implications for mixing-length models*

Both Launder & Jones (1969) and Huffman & Bradshaw (1972) have observed that an effect of acceleration is a thickening of the linear sublayer next to the wall. These investigators suggested that for predictions this thickening could be embodied in the damping factor A^+, by letting A^+ be a function of the laminarization parameter K_p or K_τ rather than a constant. In a comparable fashion, McEligot, Ormand & Perkins (1966) demonstrated that, by letting a laminar-sublayer thickness be a suitable function of local Reynolds number, good agreement could be obtained with convective heat transfer in tubes in the low-Reynolds-number range studied by Patel & Head (1968). Launder & Jones chose to represent the functional dependence in terms of K_p for their sink flow between inclined plates. Using a van Driest turbulence model similar to the one used here, they systematically varied A^+ until the computed friction factor matched 0·0048, the mean value for their data.

Huffman & Bradshaw also used a van Driest model, but, rather than matching the friction factor, they required that the predicted velocity profiles match measured profiles from the wall to 20 % of the flow width (typically $y^+ \approx$ 10–1000) for various flows. These flows included fully developed duct flows, axisymmetric wall jets and boundary layers. The two empirical functions $A^+(K)$ are graphed in figure 8 for comparison. Launder & Jones presented their function in terms of K_p, whereas Huffman & Bradshaw used K_τ, but both parameters can be compared directly here because $K_p = K_\tau$ for the radial flows of this work.

In preliminary work we have used both $A^+(K)$ functions to model selected experiments of the present work. For the experiment of figure 4, with a half angle of 2° and modest acceleration, the Huffman & Bradshaw (HB) formulation overpredicted the pressure losses by about 7 %, but the Launder & Jones (LJ) formulation underpredicted them by 12 %. For another experiment, at a half-angle of 2° and greater acceleration, $K_V = 1{\cdot}2 \times 10^{-6}$, the HB formulation again overpredicted the pressure losses, but only by 3 %, whereas the LJ formulation was 16 % too low. Tentatively we conclude that the HB formulation works somewhat better, but additional investigation is warranted.

The model of Huffman & Bradshaw indicates asymptotic behaviour of A^+ near $K_p = K_\tau = 0{\cdot}025$. A large value of A^+ causes a thick viscous layer in the predictions, with infinity corresponding to completely laminar flow. Thus this trend approximately agrees with the observation that in the vicinity of $K_\tau = K_p = 0{\cdot}04$ the parameter ϕ remains close to zero. On the other hand, Launder & Jones use a linear representation of $A^+(K_p)$ so it does not imply an asymptotic laminar situation (except as $K_p \to \infty$).

6. Conclusions

Measurements of pressure distributions for sink flow between two parallel circular disks over the ranges $9{\cdot}5 \times 10^{-6} < K_V = (\nu/V^2)\,dV/dr < 2{\cdot}2 \times 10^{-4}$, $210 < R < 20700$ and $0{\cdot}048 < r = \bar{r}/\bar{t}(\bar{Q}/4\pi\bar{\nu}\bar{t})^{\frac{1}{2}} < 3{\cdot}35$ agreed with the numerical predictions for laminar flow within the estimated experimental uncertainty. At lower Reynolds numbers the numerical predictions verified the validity of the experimental technique. At higher Reynolds numbers this agreement, in conjunction with smoke-flow visualization, confirmed the stability of these converging laminar flows for acceleration parameters K_V greater than $9{\cdot}5 \times 10^{-6}$.

Experiments were conducted for turbulent flow between parallel plates, with a sharp-cornered entry and lateral convergence due to adjustable edge walls, over the

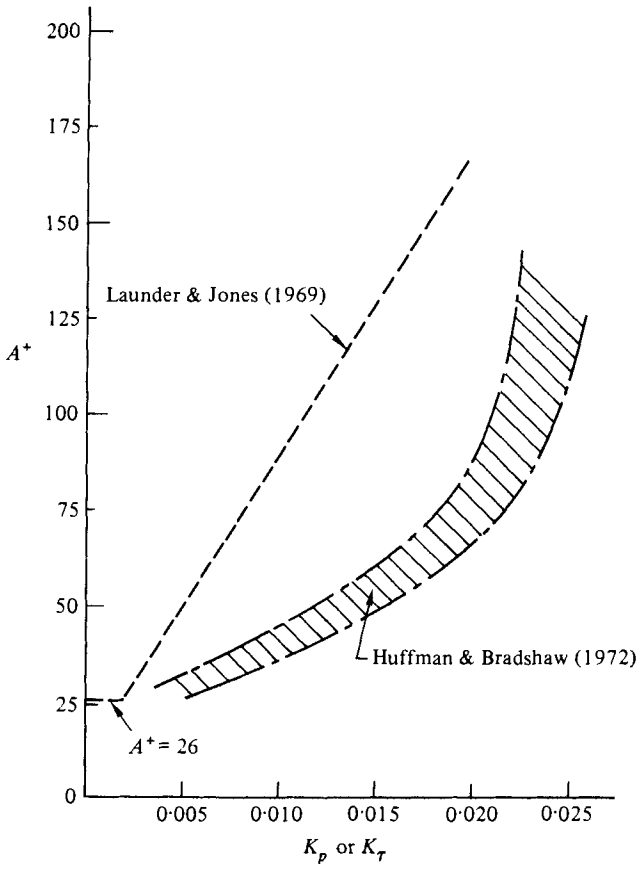

FIGURE 8. Comparison of $A^+(K_p$ or $K_\tau)$ functions.

following ranges: $1590 < Re < 68400$ and $0{\cdot}05 < r < 0{\cdot}74$. Lateral strain-rate ratios varied from -0.0003 to -0.006, giving a range of acceleration of $2{\cdot}6 \times 10^{-8} < K_V < 1{\cdot}1 \times 10^{-5}$, owing to the convergence. A numerical analysis was extended to include the van Driest (1956) mixing-length model; comparison with measured pressure distributions and local wall shear stresses showed:

(i) agreement with turbulent predictions if

$$K_V \gtrsim 10^{-7} \quad \text{or} \quad K_p = K_\tau \gtrsim 0{\cdot}003;$$

(ii) agreement with laminar predictions when

$$K_V \lesssim 4 \times 10^{-6} \quad \text{or} \quad K_p = K_\tau \lesssim 0{\cdot}04,$$

where the other acceleration parameters are defined as $K_p = (\nu/\rho u_*^3)\,dP/dr$ and $K_\tau = (\nu/\rho u_*^3)(\partial\tau/\partial z)_w$. The criteria based on K_V or K_τ are in approximate agreement with values found by other investigators for flows accelerating in geometries differing from the present experiment. It appears that K_p is a less-useful criterion, since its limiting values appear to vary significantly from one flow geometry to another. Empirical adjustment of the van Driest parameter A^+ to form a function $A^+(K_p)$, as plotted in figure 8, can yield numerical predictions in essential agreement with the measurements for laminar flows and the intermediate flows, defined as laminarizing by some investigators, as well as the turbulent experiments.

Work at the University of Arizona was supported by their Engineering Experiment Station and the National Science Foundation, whereas work at Los Alamos National Laboratory was supported by the Department of Energy and its predecessors.

REFERENCES

BADRI NARAYANAN, M. A. & RAMJEE, V. 1969 On the criteria for reverse transition in a two-dimensional boundary layer flow. *J. Fluid Mech.* **35**, 225–241.

BANKSTON, C. A. & MCELIGOT, D. M. 1970 Turbulent and laminar heat transfer to gases with varying properties in the entry region of circular ducts. *Int. J. Heat Mass Transfer* **13**, 319–344.

BELLHOUSE, B. J. & SCHULTZ, D. L. 1966 Determination of mean and dynamic skin friction, separation and transition in low-speed flow with a thin-film heated element. *J. Fluid Mech.* **24**, 379–400.

BLACKWELDER, R. F. & KAPLAN, R. E. 1976 On the wall structure of the turbulent boundary layer. *J. Fluid Mech.* **76**, 89–112.

BLACKWELDER, R. F. & KOVASZNAY, L. S. G. 1972 Large scale motion of a turbulent boundary layer during relaminarization. *J. Fluid Mech.* **53**, 61–83.

BRADSHAW, P. 1969 A note on reverse transition. *J. Fluid Mech.* **35**, 387–390.

BRADSHAW, P. 1975 Review – Complex turbulent flows. *Trans A.S.M.E.* I: *J. Fluids Engng* **97**, 146–154.

BRADSHAW, P. 1976 Complex turbulent flows. In *Theoretical and Applied Mechanics* (ed. W. T. Koiter), p. 103. North-Holland.

BROWN, G. L. 1967 Theory and application of heated films for skin friction measurments. In *Proc. Heat Transfer and Fluid Mech. Inst., University of California at San Diego.* Stanford University Press.

CHAMBERS, F. W., MURPHY, H. D. & MCELIGOT, D. M. 1983 Laterally converging flow. Part 2. Temporal wall shear stress. *J. Fluid Mech.* **127**, 403–428.

DRIEST, E. R. VAN 1956 On turbulent flow near a wall. *J. Aerospace Sci.* **23**, 1007–1011 and 1036.

FREYMUTH, P. 1977 Frequency response and electronic testing for constant temperature hot-wire anemometers. *J. Phys.* E: *Sci. Instrum.* **10**, 705–710.

HARNETT, J. P., KOH, J. C. Y. & MCCOMAS, S. T. 1962 A comparison of predicted and measured friction factors for turbulent flows through rectangular ducts. *Trans. A.S.M.E.* C: *J. Heat Transfer* **84**, 82–88.

HUFFMAN, G. D. & BRADSHAW, P. 1972 A note on von Kármán's constant in low Reynolds number turbulent flows. *J. Fluid Mech.* **53**, 45–60.

JONES, W. P. & LAUNDER, B. E. 1972 Some properties of sink-flow turbulent boundary layers. *J. Fluid Mech.* **56**, 337–351.

KAYS, W. M. & CRAWFORD, M. E. 1980 *Convective Heat and Mass Transfer*, 2nd edn. McGraw-Hill.

KLINE, S. J. 1967 Observed structure features in turbulent and transitional boundary layers. In *Fluid Mechanics of Internal Flow* (ed. G. Sovran), pp. 27–79. Elsevier.

KLINE, S. J. & MCCLINTOCK, F. A. 1953 Describing uncertainties in single-sample experiments. *Mech. Engng* **75**, 3–8.

KLINE, S. J., REYNOLDS, W. C., SCHRAUB, F. A. & RUNSTADLER, P. W. 1967 The structure of turbulent boundary layers. *J. Fluid Mech.* **30**, 741–773.

LAUNDER, B. E. & JONES, W. P. 1969 Sink flow turbulent boundary layers. *J. Fluid Mech.* **38**, 817–831.

LAUNDER, B. E. & STINCHCOMBE, H. S. 1967 Non-normal similar turbulent boundary layers. *Imperial Coll. Mech. Engng Tech. Rep.* TWF/TN 21.

MCELIGOT, D. M. 1963 The effect of large temperature gradients on turbulent flow of gases in the downstream region of tubes. Ph.D. thesis, Stanford University, TID-19446.

MCELIGOT, D. M., COON, C. W. & PERKINS, H. C. 1970 Relaminarization in tubes. *Int. J. Heat Mass Transfer* **13**, 431–433.

MCELIGOT, D. M., ORMAND, L. W. & PERKINS, H. C. 1966 Internal low Reynolds number turbulent and transitional gas flow with heat transfer. *Trans. A.S.M.E.* C: *J. Heat Transfer* **88**, 239–245.

MURPHY, H. D. 1979 Flow near the outlet of a geothermal energy reservoir. Ph.D. thesis, University of Arizona. Also *Report* LA-7906-T, available from the National Technical Information Service.

NARASIMHA, R. & SREENIVASAN, K. R. 1973 Relaminarization in highly accelerated turbulent boundary layers. *J. Fluid Mech.* **61**, 417–447.

NARASIMHA, R. & SREENIVASAN, K. R. 1979 Relaminarization of fluid flows. *Adv. Appl. Mech.* **19**, 221–309.

PATEL, V. C. 1965 Calibration of the Preston tube and limitations on its use in pressure gradients. *J. Fluid Mech.* **23**, 185–208.

PATEL, V. C. & HEAD, M. R. 1968 Reversion of turbulent to laminar flow. *J. Fluid Mech.* **34**, 371–392.

SHAW, R. 1960 The influence of hole dimensions on static pressure measurements. *J. Fluid Mech.* **7**, 550–564.

SMITS, A. J., EATON, J. A. & BRADSHAW, P. 1979 The response of a turbulent boundary layer to lateral divergence. *J. Fluid Mech.* **94**, 243–268.

WORSOE-SCHMIDT, P. M. 1967 Heat transfer in the thermal entrance region of circular tubes and annular passages with fully developed laminar flow. *Int. J. Heat Mass Transfer* **10**, 541–551.